DOI: https://doi.org/10.14256/JCE.4413.2025

Građevinar 7/2026

Primljen / Received: 30.9.2025.
Ispravljen / Corrected: 9.4.2026.
Prihvaćen / Accepted: 19.6.2026
Dostupno online / Available online: 10.8.2026.

Study of the mechanical properties of desert sand basalt fiber concrete for hydraulic structures

Authors:

[1,2]**Jianpeng Zhang**, MCE
17041@ylnu.edu.cn
Corresponding author

[1]**Xiaodi Dong**, MCE
dxd4244DXD@163.com

[3]**Han Xu**, MCE
bicycle987@163.com

[1]**Qingsong Li**, MCE
Lqs1944717024@163.com

[1] **Yifan Han**, MCE
m15099196374@163.com

[1] Yili Normal University, China
Faculty of Physical Science and Technology
[2] Xinjiang Condensed Matter Phase Transition and Microstructure Laboratory, China
[3] Yili Hongjing Engineering Detection Co., China

Research Paper

Jianpeng Zhang, Xiaodi Dong, Han Xu, Qingsong Li, Yifan Han

Study of the mechanical properties of desert sand basalt fiber concrete for hydraulic structures

In this study, basalt fibres and desert sand were mixed into concrete for hydraulic structures, and their impact on the mechanical characteristics and cost was investigated. The experiment was designed as an orthogonal test, where the water-cement ratio, fly ash replacement rate, desert sand replacement rate, and amount of basalt fibres were varied to assess the mechanical properties of desert sand basalt fibre concrete (DSBFC). The microstructure and physical phase composition of DSBFC were studied using scanning electron microscopy and X-ray diffraction. The results suggest that the water-cement ratio and fly ash replacement rate are the primary factors influencing the mechanical properties of DSBFC, while basalt fibres effectively prevent concrete cracking. The DSBFC with optimum composition, designated as A1B2C2D2, comprised a water-cement ratio of 0.5, fly ash replacement ratio of 5 %, desert sand replacement ratio of 10 %, and basalt fibre amount of 0.5 kg/m^3. Compared with regular concrete, DSBFC increased the compressive strength, flexural strength and split tensile strength by 9.05 %, 2.72 %, and 21.60 %, respectively, and the cost of concrete per cubic meter decreased by 0.958 %.

Key words:

orthogonal tests, mechanical properties, microstructure, pozzolanic effect, desert sand, basalt fiber

Prethodno priopćenje

Jianpeng Zhang, Xiaodi Dong, Han Xu, Qingsong Li, Yifan Han

Ispitivanje mehaničkih svojstava betona s pustinjskim pijeskom i bazaltnim vlaknima za hidrotehničke građevine

U ovome istraživanju bazaltna vlakna i pustinjski pijesak ugrađeni su u beton za hidrotehničke građevine kako bi se ispitao njihov utjecaj na mehanička svojstva i troškove proizvodnje betona. Ispitivanje je provedeno primjenom ortogonalnoga eksperimentalnog plana u kojemu su mijenjani omjer vode i cementa, udio zamjene cementa letećim pepelom, udio zamjene riječnog pijeska pustinjskim pijeskom te količina bazaltnih vlakana radi procjene mehaničkih svojstava betona s pustinjskim pijeskom i bazaltnim vlaknima (DSBFC). Mikrostruktura i fazni sastav DSBFC-a analizirani su primjenom pretražnoga elektronskog mikroskopa (SEM) i rendgenske difrakcije (XRD). Rezultati pokazuju da su omjer vode i cementa te udio letećeg pepela glavni čimbenici koji utječu na mehanička svojstva DSBFC-a, dok bazaltna vlakna učinkovito sprječavaju nastanak pukotina u betonu. Optimalni sastav DSBFC-a, označen kao A1B2C2D2, obuhvaća omjer vode i cementa od 0,50, zamjenu cementa letećim pepelom od 5 %, zamjenu riječnog pijeska pustinjskim pijeskom od 10 % te dodatak bazaltnih vlakana u količini od 0,5 kg/m^3. U usporedbi s običnim betonom, optimalni DSBFC povećao je tlačnu čvrstoću za 9,05 %, čvrstoću na savijanje za 2,72 % te vlačnu čvrstoću cijepanjem za 21,60 %, dok su troškovi proizvodnje kubnog metra betona smanjeni za 0,958 %.

Ključne riječi:

ortogonalni pokusi, mehanička svojstva, mikrostruktura, pucolanski učinak, pustinjski pijesak, bazaltna vlakna

1. Introduction

The Xinjiang region has unique natural ecological characteristics, including a high salt content, cold temperatures, high seismic activity, and large daily temperature differences [1-3]. Hydraulic engineering is therefore crucial for the economic and social development of this region [4]. However, over time, hydraulic engineering systems in this region have been exposed to high-intensity earthquakes and frequent freeze-thaw cycles. Consequently, concrete structures are susceptible to issues such as cracks, spalling, carbonisation, internal reinforcement corrosion, and channel leakage. Additionally, freezing and expansion forces cause lining plates to bulge, fracture, and collapse, posing significant threats to the development of Xinjiang's economy and society [5-9]. Therefore, there is an urgent need to develop concrete materials capable of repairing damaged sections in hydraulic engineering structures.

Basalt fibre is a type of inorganic fibre derived from natural basalt that exhibits favourable qualities, such as high strength, elasticity modulus, corrosion resistance, and temperature resistance [10, 11]. Its use in concrete and mortar has gained popularity as it can effectively limit fracture formation and expansion while improving crack resistance and toughness in concrete via bridging, crack blocking, and stress transfer [12-14]. Huang et al. [15] investigated the impact of varying fibre lengths (3, 6, 9, and 12 mm) on concrete and reported that concrete with 6 mm basalt fibres had superior mechanical properties and frost resistance. Qin et al. [16] studied basalt fibres with lengths of 6, 24, 30, and 48 mm. Their results indicate that 24 mm basalt fibres can effectively enhance the internal void structure of concrete, restrict the formation of microcracks, and increase densification, thereby improving the mechanical properties of concrete. Krassowska [17] and Wang [18] found that the inclusion of 12 and 24 mm short-cut basalt fibres in concrete beams and columns delayed crack initiation and significantly diminished crack formation and severity. Researchers have also reported on the use of basalt fibres in recycled aggregate concrete [19, 20], gangue concrete [21], coral aggregate concrete [22], and pumice-based foam concrete [23].

Desert sand, a widely dispersed but underutilised natural resource in Xinjiang, is typically considered unsuitable for direct use in construction projects because of its fine particle size, poor gradation, and high silt content [24]. However, with depleting natural river sand resources and increasing environmental protection needs, the use of desert sand resources has emerged as a research hotspot [25, 26]. Zhang et al. [27] employed desert sand to create ultrahigh-performance alkali-activated concrete. Xu et al. [28] studied the mechanical characteristics of desert sand concrete under dry-wet cycling and sulphate attack. Munir et al. [29] discovered that the compression casting of desert-sand concrete might produce better mechanical qualities and durability. Farida [30] produced self-compacting concrete from desert sand and investigated its flow, mechanical characteristics, and durability. Several experimental studies on the application of steel, glass, and polypropylene fibres in desert-sand concrete have also been conducted [31-33].

In recent years, energy conservation and sustainable construction have become central themes in civil engineering. Fly ash, a large-volume by-product of coal-fired power generation, is widely used as a supplementary cementitious material. Notably, its inclusion reduces the concrete production costs and contributes significantly to environmental protection [34, 35]. Zehra et al. [36] developed a self-compacting lightweight concrete using fly ash and basalt fibres. Fly ash improved flowability and long-term strength, whereas basalt fibre enhanced tensile strength and crack resistance. Their synergistic effects optimised microstructures and durability of self-compacting lightweight concrete. In addition, Li et al. [37] found that the co-incorporation of fly ash and basalt fibre into concrete promoted the secondary hydration of cementitious materials, enhanced the matrix compactness, and improved the fibre-matrix bonding. This synergy allows basalt fibres to be more effectively encased within the hardened matrix, thus forming a cooperative load-bearing mechanism. Hamada et al. [38] prepared high-strength concrete by blending fly ash, granulated blast-furnace slag, and desert sand, fully utilising the filling and pozzolanic effects of fly as; the resulting mix achieved a 7 days compressive strength of 76.45 MPa. Zhang et al. [39] employed fly ash and desert sand to produce lightweight concretes with strength grades LC20 and LC25.

Although basalt fibre concrete and desert sand concrete have been extensively researched, studies on desert sand basalt fibre concrete (DSBFC) remain scarce. This study examines the influence of the water-cement ratio, fly ash replacement ratio, desert sand replacement ratio, and basalt fibre amount on the workability, mechanical properties, microstructure, and physical phase composition of concrete through orthogonal tests, ultimately identifying the optimal formulation of DSBFC suitable for repairing damaged hydraulic concrete structures.

2. Raw materials and experimental design

2.1. Raw materials

The raw materials included P.O 42.5R cement manufactured by Xinjiang Zhongtai Chemical Torkun Energy Chemical Co., Ltd. (Table 1) and Class II fly ash manufactured by the Xinjiang Hengtai Bailian New Material Technology Co., Ltd. (Table 2). The aggregates used were (1) river sand, which was coarse sand with fineness modulus of 3.34, moisture content of 5.46 %, apparent density of 2640 kg/m^3, and a

Table 1. Physical and mechanical properties of P.O 42.5R cement

Density [g/cm³]	**Specific surface area** [m²/kg]	**Setting time** [min]		**Flexural strength** [MPa]		**Compressive strength** [MPa]	
		Initial	**Final**	**3 days**	**28 days**	**3 days**	**28 days**
3.1	362.5	170	218	6.6	9.2	31.3	56.5

Table 2. Physical properties of Class II fly ash

Fineness [%]	**Loss on ignition** [%]	**Water demand ratio** [%]	**Moisture content** [%]
7.7	3.91	95	0.3

Table 3. Parameters of the basalt fibre

Diameter [μm]	**Density** [g/cm³]	**Elongation** [%]	**Tensile strength** [MPa]	**Elasticity modulus** [MPa]
7 – 15	2.65	2.8	4000	105

particle size range of 0-4.75 mm; and (2) desert sand, with fineness modulus of 0.8, apparent density of 2663 kg/m³, and a particle size range of 0-0.4 mm. Both aggregates conformed to the particle grading criteria outlined in JGJ 52 [40] and ASTM C33 [41], as illustrated by the sieve analysis curves shown in Figure 1.

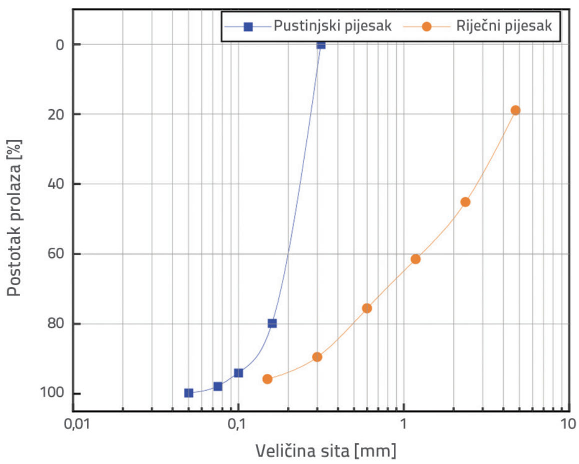

Figure 1. Particle size distribution curves of desert sand and river sand

Short-cut basalt fibres measuring 12 mm in length were obtained from Xinjiang Woyu Preventive and Control New Materials Company, Ltd. (Table 3). HSC polycarboxylic acid was used as a water-reducing agent and demonstrated a water reduction ratio of 15 wt percent. Municipal tap water was used for the experiments.

2.2. Orthogonal experimental design

The orthogonal test method is a multifactor optimisation experimental design technique utilizing an orthogonal table; this design significantly decreases the number of tests required and effectively evaluates the influence of factors through the scientific selection of representative test combinations [42]. In this study, C40 concrete (design strength class of 40 MPa) for hydraulic structures was selected as the research object. Four factors were investigated: the water-cement ratio (W/C), fly ash replacement ratio (FA), desert sand replacement ratio (DS), and basalt fibre amount (BF). Each factor was assigned four levels, and the mix proportions were calculated based on JGJ 55-2011 [43]. Specifically, FA level 1 denotes no FA replacement, DS level 1 indicates fine aggregates from river sand, and BF level 1 represents zero BF dosage. The factors and their levels are listed in Table 4, and the orthogonal test mix proportions are listed in Table 5. In the coding scheme, A, B, C, and D correspond to the W/C, FA, DS, and BF, respectively.

Table 4. Factors and levels of mix proportion design

Level	**W/C**	**FA** [%]	**DS** [%]	**BF** [g/cm³]
	A	**B**	**C**	**D**
1	0.50	0	0	0
2	0.55	5	10	0.5
3	0.60	10	20	1.0
4	0.65	15	30	1.5

2.3. Specimen production and test methods

To prepare specimens, river sand and desert sand were first added to the mixer and stirred for 30 s, followed by cement and fly ash for 2 min, basalt fibre for 1 min, and finally water and a water reduction agent for 8 min. Subsequently, the specimen mould was poured, placed on a vibration table, and the concrete surface smoothed and finished. Figure 2 shows a flowchart of the specimen production process. The compressive and splitting tensile strengths were tested at 3, 7, 28 and 56 days, using 24 specimens measuring 100 × 100 × 100 mm, and the flexural

Table 5. Orthogonal test mix proportions [g/cm³]

Number	Mixture code	Water	Cement	Fly ash	Desert sand	River sand	Basalt fibre	Water reducer	Density
1	A1B1C1D1	290	580	0	0	1298	0	1.16	2169.16
2	A1B2C2D2	290	551	29	130.64	1165.65	0.5	1.16	2167.95
3	A1B3C3D3	290	522	58	260.72	1033.86	1	1.16	2166.74
4	A1B4C4D4	290	493	87	390.22	902.65	1.5	1.16	2165.53
5	A2B1C2D3	290	527.27	0	135.61	1209.96	1	1.05	2164.89
6	A2B2C1D4	290	500.91	26.36	0	1341.82	1.5	1.05	2161.64
7	A2B3C4D1	290	474.55	52.73	405.27	937.47	0	1.05	2161.07
8	A2B4C3D2	290	448.18	79.09	269.66	1069.33	0.5	1.05	2157.81
9	A3B1C3D4	290	483.33	0	279.02	1106.45	1.5	0.97	2161.27
10	A3B2C4D3	290	500.91	26.36	417.82	966.49	1	0.97	2203.55
11	A3B3C1D2	290	474.55	52.73	0	1378.34	0.5	0.97	2197.09
12	A3B4C2D1	290	448.18	79.09	138.80	1238.38	0	0.97	2195.42
13	A4B1C4D2	290	446.15	0	428.44	991.04	0.5	0.89	2157.02
14	A4B2C3D1	290	423.85	22.31	285.18	1130.88	0	0.89	2153.11
15	A4B3C2D4	290	401.54	44.62	142.37	1270.28	1.5	0.89	2151.20
16	A4B4C1D3	290	379.23	66.92	0	1409.24	1	0.89	2147.28

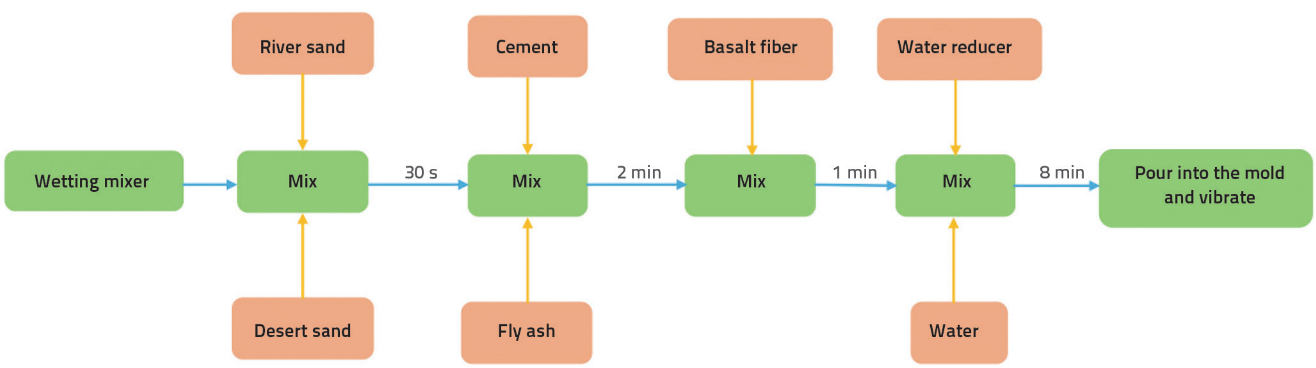

Figure 2. Flowchart of specimen preparation process

strength was tested at 7 and 28 days using six specimens measuring 160 × 40 × 40 mm. After 1 day, the specimens were demoulded and placed in a normal curing box for 28 dayd.

During the stirring phase, the basalt fibres transitioned from flaky bundles to monofilaments via friction and ripping between the mortar aggregates, as illustrated in Figure 3. The tearing of the chopped basalt fibres improved as stirring time increased. Finally, chopped basalt fibres were added and mixed for 8 min. After tearing, the basalt monofilaments were more uniformly dispersed in the mortar.

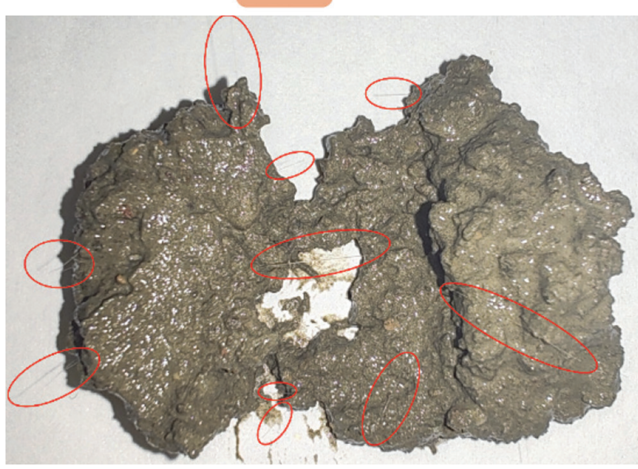

Figure 3. Basalt fibre monofilament state after mixing

Slump test procedure:

1. The slump cone was filled with three layers of uniformly mixed concrete, with each layer occupying approximately one-third of the cone volume. Each layer was then compacted with 25 tamps using a standard rod, applied in a spiral manner from the edge toward the centre. For the top layer, supplementary concrete was added as required to ensure that the cone was completely filled.
2. After completing the concrete filling, the surface was levelled by scraping off the excess concrete with a trowel and smoothing the cone mouth.
3. The slump cone was lifted vertically and steadily, and then placed beside the slumped specimen. The height of the cone and the highest point of the slumped specimen were measured, and the difference between the two values was recorded as the slump.

The compressive and splitting tensile strengths were measured at 3, 7, 28 and 56 days, and the flexural strength was tested at 7d and 28d, in accordance with SL/T 352-2020 [44]. The workability of the concrete for hydraulic structures was assessed following GB/T 50080-2016 [45]. Each reported strength value represents the arithmetic mean of three specimens per group. The loading rate was controlled at 0.5 to 0.8 MPa/s for compressive strength tests and 0.05 to 0.08 MPa/s for splitting tensile strength tests. Because the compressive and splitting tensile specimens of the DSBFC were cubes measuring 100 × 100 × 100 mm, rather than the standard 150 × 150 × 150 mm, correction factors were applied to the results. Specifically, the compressive strength was multiplied by 0.95 and the splitting tensile strength was multiplied by 0.85.

2.4. Scanning electron microscope (SEM) and X-ray diffraction (XRD) tests

Scanning electron microscopy (SEM) was performed using a ZEISS Sigma 500 scanner. Concrete samples with 5 mm thickness were selected and immersed in ethylene glycol for 48 h. The glycol solution was then replaced, and the samples were immersed for an additional 48 h. Subsequently, the samples were removed, dried, sputter-coated with gold, and examined by SEM to determine their microscopic morphology. X-ray diffraction (XRD) was performed using a Bruker-D8 ADVANCE machine manufactured in Germany. Concrete specimens of different curing ages, previously dehydrated by ethylene glycol treatment, were oven-dried at 65 °C until constant weight was achieved. The dried samples were ground in a mortar and passed through a 200-mesh sieve (particle size ≤ 0.075 mm). The resulting powder was subjected to XRD analysis. Scanning was performed over a 2θ range of 5 to 65° at a rate of 5°/min.

3. Test results

Test results for the mechanical properties of DSBFC are presented in Table 6, and the slump test results are displayed in Table 7.

At 28d, the splitting tensile strength of each group was approximately 7.27 to 9.47 % of the cube compressive strength, which was consistent with the performance

Table 6. Test results of the mechanical properties of DSBFC

Number	Compressive strength [MPa]				Flexural strength [MPa]		Splitting tensile strength [MPa]			
	3d	7d	28d	56d	7d	28d	3d	7d	28d	56d
1	46.89	50.33	53.37	56.65	3.05	3.67	2.95	3.80	4.12	4.45
2	48.26	55.48	58.20	61.11	3.08	3.77	2.64	3.82	5.01	6.20
3	37.95	47.72	56.23	59.26	2.92	3.63	2.86	3.80	4.92	5.06
4	30.78	45.36	47.00	51.27	2.75	3.14	2.54	2.92	4.26	4.92
5	34.27	47.05	51.50	53.93	3.13	3.52	3.06	3.58	4.31	4.94
6	35.21	48.48	54.20	57.11	3.24	3.66	3.01	3.56	4.53	5.04
7	28.13	37.99	42.67	44.80	2.81	3.34	2.05	3.28	3.91	3.99
8	26.81	37.71	43.07	45.22	2.76	3.28	2.10	3.04	3.46	4.21
9	32.33	39.50	45.20	47.31	2.47	3.31	2.67	3.11	3.91	4.66
10	28.97	37.70	45.63	48.62	2.78	3.54	2.56	3.06	3.55	4.36
11	37.76	48.18	51.80	54.53	3.29	3.50	2.66	3.20	4.05	4.56
12	37.34	47.85	50.90	54.24	3.17	3.30	2.53	3.18	3.94	4.89
13	28.21	35.01	50.80	52.29	2.52	3.48	2.03	2.59	3.76	4.52
14	26.46	35.29	51.00	53.34	2.48	3.53	2.04	3.15	3.71	4.96
15	28.49	38.14	43.90	46.10	2.65	3.40	1.96	2.90	3.43	4.65
16	24.54	35.42	41.20	43.90	2.41	3.02	1.78	3.11	3.90	4.11

Table 7. Experimental results of slump test for DSBFC

Number	1	2	3	4	5	6	7	8	9	10	11	12	13	14	15	16
Slump [mm]	116	130	156	164	134	124	150	139	108	146	104	143	129	130	114	126

of ordinary concrete. The flexural strength ranged from approximately 6.46 to 7.83 % of the compressive strength. In all cases, it was lower than the split tensile strength. This difference is attributed to the specimen geometry. Flexural tests were performed on mortar prisms with dimensions of 40 × 40 × 160 mm, whose smaller size generally yielded lower measured strength values.

4. Analysis of test results

4.1. Work performance analysis

During the test, after the slump cylinder was lifted, the concrete in each group formed a small upper cone and large lower cone when it fell, as illustrated in Figure 4. Tapping its side caused the concrete cone to fall gently without collapsing or partially crumbling, and no dilute cement paste emerged around the bottom of the concrete, suggesting that the concrete had good cohesiveness and moisture retention. The slump values reported in Table 7 ranged between 104 to 164 mm, with most results falling within the 100 to 160 mm range. These values indicate that DSBFC samples exhibit high workability, thereby satisfying the engineering and construction requirements. The presence of basalt fibre monofilaments enhanced the internal cohesion compared with ordinary concrete, as the fibres provided additional resistance against segregation [46].

Figure 4. Slump of DSBFC

4.2. Mechanical properties analysis

4.2.1. Type of failure

Cubic compressive strength tests were conducted on the DSBFC specimens, and their failure morphologies are shown in Figure 5. At the start of loading, the specimen showed no visible change in appearance, and its internal structure remained the same. Upon reaching 50 to 70 % of the ultimate strength, microcracks were initiated from the edges, corners, or interior weak points of the specimen. As the stress increased, the microcracks gradually enlarged and merged, forming a main crack that extended diagonally across the specimen, leading to the development of a shear surface. Near the ultimate load, the primary crack rapidly extended, leading to a sudden loss of stability. Subsequently, the specimen failed abruptly, accompanied by a distinct cracking sound.

Figure 5. Failure morphology of DSBFC under compressive loading

The damage observed during the flexural strength tests is shown in Figure 6. During the initial stage of loading, the appearance and internal structure of the specimen remained unchanged. When the load applied reached 50 to 70 % of the ultimate strength, microcracks were initiated at the midspan along the bottom surface. These microcracks propagate upward within a limited zone. With further loading, the microcracks extended vertically, their widths increased, and noticeable cracks appeared on the bottom surface. As the load approached its maximum value, the fractures expanded rapidly and abruptly and were accompanied by distinct cracking sounds. Examination of the fracture surface revealed exposed basalt fibre monofilaments, indicating that the fibres were pulled out rather than broken, confirming their crack-bridging role.

Figure 6. Flexural strength failure morphology of DSBFC

The splitting tensile strength test results are shown in Figure 7. At the beginning of loading, the specimen showed no visible change. When the load reached 50 to 70 % of the ultimate strength, a slight deformation occurred in the compressed zone and microcracks were formed in the central region. These cracks propagated downward along the loading axis. As the strain increased, the microcracks extended further and one dominant crack soon penetrated the specimen, producing audible cracking sounds.

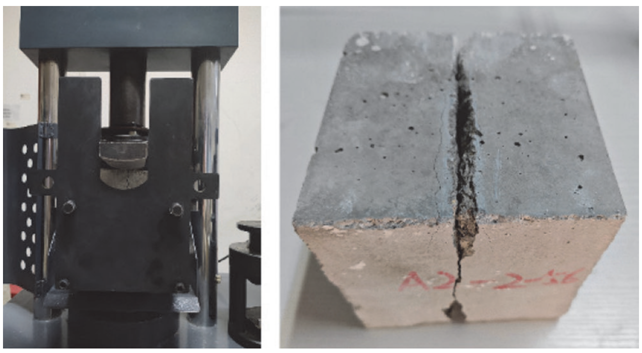

Figure 7. Splitting tensile strength failure morphology of DSBFC

Figure 8. Splitting tensile failure surface of DSBFC

As shown in Figure 8, even after a complete fracture occurred during the splitting tensile test, the basalt fibres continued to bridge the two separated halves of the specimen. The fibres were pulled out rather than ruptured, indicating that their tensile capacity was not exceeded. This behaviour is consistent with the performance of basalt fibres observed in the flexural strength tests.

4.2.2. Analysis of mechanical properties

Figure 9 shows the cubic compressive strength results for each group.

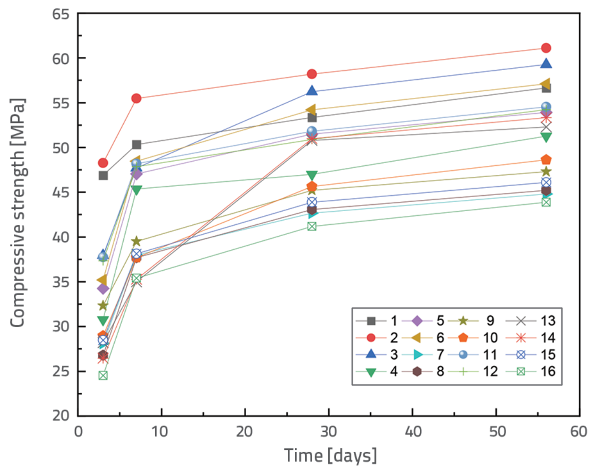

Figure 9. Cubic compressive strength of DSBFC

The strength increased with curing age across all samples. The rate of strength gain was rapid from 0 to 28d, whereas the growth between 28 to 56 days declined significantly. By 28 day, the specimens had already achieved 95 % of their 56 days strength. At 56 day, Group 2 recorded the highest compressive strength at 61.11 MPa, whereas Group 16 exhibited the lowest at 41.62 MPa. Notably, the 7d strengths of Groups 3 and 6 were lower than those of the control group (Group 1); however, by 28d, both exceeded those of the control group. Additionally, the strength growth rates of Groups 13 and 14 were 45.1 % and 44.5 %, respectively. This enhancement can be attributed to cement hydration during the early curing period (0-7d), which generates a substantial quantity of calcium hydroxide. Subsequently, fly ash reacts with the generated calcium hydroxide to form a calcium silicate hydrate (C-S-H) gel, thereby densifying the concrete matrix and accelerating strength development [47,48].

Figure 10 shows the prismatic flexural strength results for each group.

The flexural strength increased with the curing age for all groups. At 28d, Group 2 achieved the highest flexural strength at 3.77 MPa, whereas Group 16 recorded the lowest at 3.02 MPa. Between 7d-28d, Groups 14 and 16 exhibited relatively rapid strength growth, with increases of up to 42.3 %.

Figure 11 shows the splitting tensile strength results for each group.

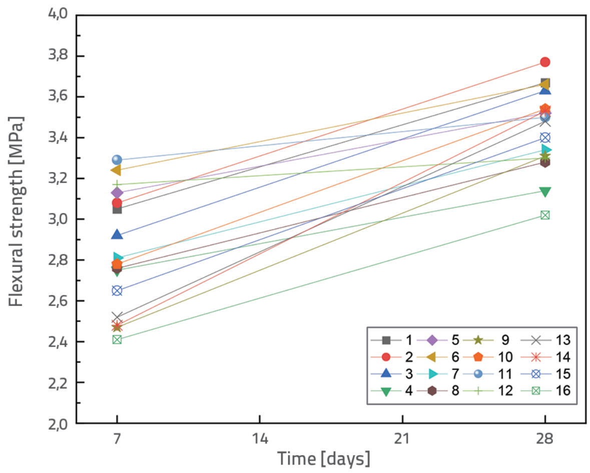

Figure 10. Prismatic flexural strength of DSBFC

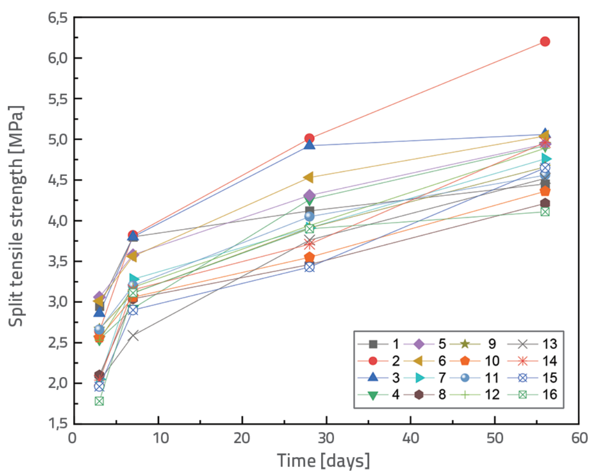

Figure 11. Cubic splitting tensile strength of DSBFC

Similar to the compressive and flexural strengths, the splitting tensile strength increased with the curing age. At 56d, Group 2 achieved the maximum splitting tensile strength at 6.20 MPa, whereas Group 16 demonstrated the lowest value at 3.11 MPa, aligning with their compressive strength performance.

4.2.3. Stochastic analysis

The compressive, flexural, and splitting tensile strengths at 28d were statistically evaluated using the online software SPSS (https://spssau.com). In this analysis, a higher R value for the extreme difference indicates a stronger influence of the corresponding factor on the experimental outcomes. The range analysis results are presented in Table 8.

The results indicate significant differences among the influencing factors. For the 28 days compressive strength, the order of influence was FA > W/C > DS > BF. For the 28 days flexural strength, the ranking was FA > W/C > BF > DS. For the 28 days splitting tensile strength, the ranking was W/C > FA > DS > BF.

4.3. Optimal ratio determination

To illustrate the correlation between the mechanical properties of DSBFC and the varying levels of each factor, the factor levels were plotted on the horizontal axis, with the 28 days mechanical strength on the vertical axis. The resulting diagrams presented in Figures 12 to 14 depict the relationships between the factor levels and strength indices, thereby providing a visual basis for determining the optimal mix ratio.

As shown in Figure 12, the compressive strength of the DSBFC decreased progressively with increasing W/C. Specifically, at a W/C of 0.65, the compressive strength decreased by 13.4 % compared with that at 0.5. A higher W/C increased the concentration of free water molecules. As curing progressed, the evaporation of these molecules left voids in the concrete mix, which reduced the structural compactness and strength. Thus, higher W/Cs correlate with greater void formation

Table 8. Range analysis results

Number	28d compressive strength [MPa]				28d flexural strength [MPa]				28d splitting tensile strength [MPa]			
	A	B	C	D	A	B	C	D	A	B	C	D
k1j	53.95	50.22	51.14	49.48	3.55	3.50	3.46	3.46	4.58	4.03	4.15	3.92
k2j	48.86	53.26	51.13	50.97	3.45	3.62	3.50	3.51	4.05	4.20	4.17	4.07
k3j	48.38	48.90	49.13	48.89	3.41	3.47	3.44	3.43	3.86	4.08	4.00	4.17
k4j	46.72	45.54	46.53	48.58	3.36	3.18	3.38	3.38	3.70	3.89	3.87	4.03
R	7.23	7.71	4.62	2.39	0.20	0.44	0.12	0.13	0.88	0.31	0.30	0.25

Note: k1j represents the mean of the results of the tests in column j related to factor level 1; R is the extreme variance.

and lower compressive strength. Numerous studies have confirmed the inverse relationship between the W/C and compressive strength [49, 50].

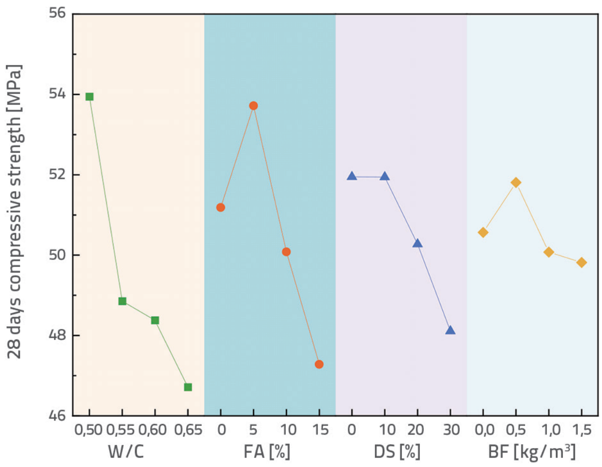

Figure 12. Compressive strength range diagram. W/C, water-cement ratio; FA, fly ash replacement ratio; DS, desert sand replacement ratio; and BF, basalt fibre amount

The addition of fly ash changed the compressive strength of the concrete. At 5 % FA, the compressive strength increased by 6.05 % compared with that of the control group. However, when the fly ash content exceeded 10 %, the concrete strength decreased compared with that of the control group. This effect is attributed to the interaction of fly ash within the concrete mixture. At lower fly ash levels, it reacts with calcium hydroxide (a cement hydration byproduct) to form a C-S-H gel, which densifies the matrix and enhances its strength [51]. At higher fly ash levels, all the available calcium hydroxide in the mixture react with fly ash; however, some fly ash remained unreacted. This unreacted fraction acts only as a microaggregate filler, reducing the effective amount of cementitious material bound to the aggregates, thereby lowering strength [52].

The particle size of desert sand is generally smaller than that of river sand. At 10 % DS, there was minimal impact on the compressive strength; however, higher DS levels caused strength reduction. This is because finer desert sand particles have larger specific surface areas than an equivalent mass of river sand. Consequently, more cement particles are required for curing, leading to a reduced distribution of the binding material among the aggregates and ultimately reducing strength.

BF also influences the compressive strength. At 0.5 kg·m^{-3} BF, the maximum compressive strength increased by 3.01 % compared with that of the control group. This enhancement is ascribed to fibre dispersion during mixing, where friction with the mortar slurry separates the fibres into monofilaments. These monofilaments disrupt void connectivity, diminish large-void formation, and enhance matrix compactness. However, when the BF content rose to 1.0 kg·m^{-3}, the compressive strength decreased by 1.19 % relative to that of the control group. This decline was attributed to high BF, which resulted in the coalescence of monofilament fibres and the creation of weak internal structures. Consequently, these regions failed prematurely, leading to specimen crushing.

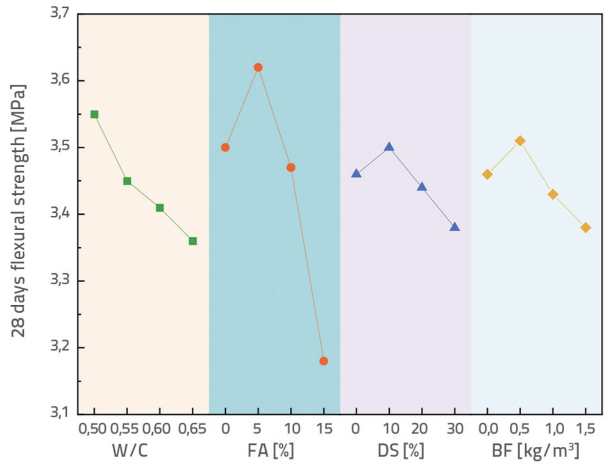

Figure 13. Flexural strength range diagram. W/C, water-cement ratio; FA, fly ash replacement ratio; DS, desert sand replacement ratio; and BF, basalt fibre amount

Figure 13 depicts the influence of the four factors on the flexural strength, which follows a trend similar to that observed for the compressive strength. At 10 % DS, the flexural strength improved compared with that of ordinary concrete. This enhancement is attributed to the fine desert sand filling the microvoids in the concrete paste, thereby increasing matrix compactness [53]. However, FA did have a significant effect. At 15 % FA, the flexural strength decreased by 9.14 % compared with that of the control group. Excessive fly ash acts primarily as an inert filler; it is unable to participate in hydration or provide bonding between aggregates and fibres, thereby reducing structural integrity.

Figure 14 shows that the effects of W/C, FA, and DS on the splitting tensile strength, compressive strength, and flexural strength were essentially the same; however, the impact of BF differed considerably. As the BF dosage increased from 0.5 to 1.5 kg·m^{-3}, the splitting tensile strength initially increased and then decreased. Maximum compressive strength was achieved at 1.0 kg·m^{-3} dosage. Among all the factors, W/C exhibited the most significant effect on the splitting tensile strength.

Table 8 and the trends shown in Figures 12-14 indicate that among the four factors, W/C and FA have a more significant effect on concrete strength, whereas BF has the least impact. The mechanical properties of the DSBFC generally deteriorate with increasing W/C, FA, and DS. Conversely, the splitting tensile strength exhibited an initial increase followed by a decrease with varying BF dosage.

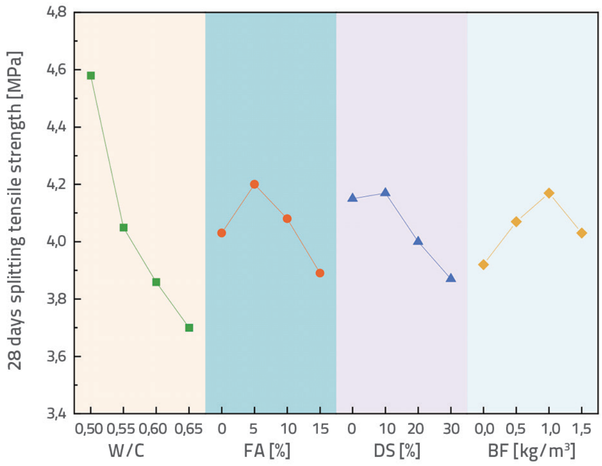

Figure 14. Splitting tensile strength range diagram. W/C, water-cement ratio; FA, fly ash replacement ratio; DS, desert sand replacement ratio; and BF, basalt fibre amount

From Figures 12-14, the following factor levels are identified as optimal: For W/C, Level 1 produced the best performance across all test indicators. For FA, level 2 yielded superior results. In the case of DS, the compressive strengths were nearly identical at levels 1 and 2 in Figure 12, but the flexural and splitting tensile strengths were the highest at level 2 in Figures 13 and 14; thus, level 2 was selected. For BF, level 2 provided the highest compressive and flexural strengths, as shown in Figures 12 and 13, respectively. Although Level 3 yielded the maximum splitting tensile strength in Figure 14, its compressive and flexural strengths in Figures 12 and 13 were lower than those of the control group, making Level 2 a more appropriate choice. In summary, the optimal mixing parameters are W/C = 0.50, FA = 5 %, DS = 10 %, and BF = 0.5 kg·m^{-3}. Compared with the control group, this mix increased the compressive, flexural, and splitting tensile strengths by 9.05 %, 2.72 %, and 21.60 %, respectively.

4.4. Microstructure analysis

4.4.1. SEM testing

SEM was used to analyse the microstructural conditions of the concrete components. A second set of specimens cured for 3 and 28 days was examined, and the corresponding micrographs are displayed in Figure 15.

At 3d, the hydrated morphology is shown in Figure 15.a, in which the basalt fibre monofilaments are visible. This observation was consistent with the flaky short-cut basalt fibre agglomerates dispersed in a monofilament state during mixing (Figure 3). C-S-H was attached to the fibres, indicating effective bonding between the slurry and basalt fibres. Figure 15.b shows Fa particles embedded in a matrix surrounded by lamellar calcium hydroxide (CH) and agglomerated flocculent C-S-H. In the locally enlarged image in Figure 15.c, needle- and rod-shaped ettringites (Aft) are clearly observed.

At 28d, Figure 15.d reveals a dense C-S-H-dominated reticulated morphology that tightly interconnects the matrix. The magnified view in Figure 15.e clearly shows C-S-H in a three-dimensional mesh distribution along with lamellar CH, both of which are

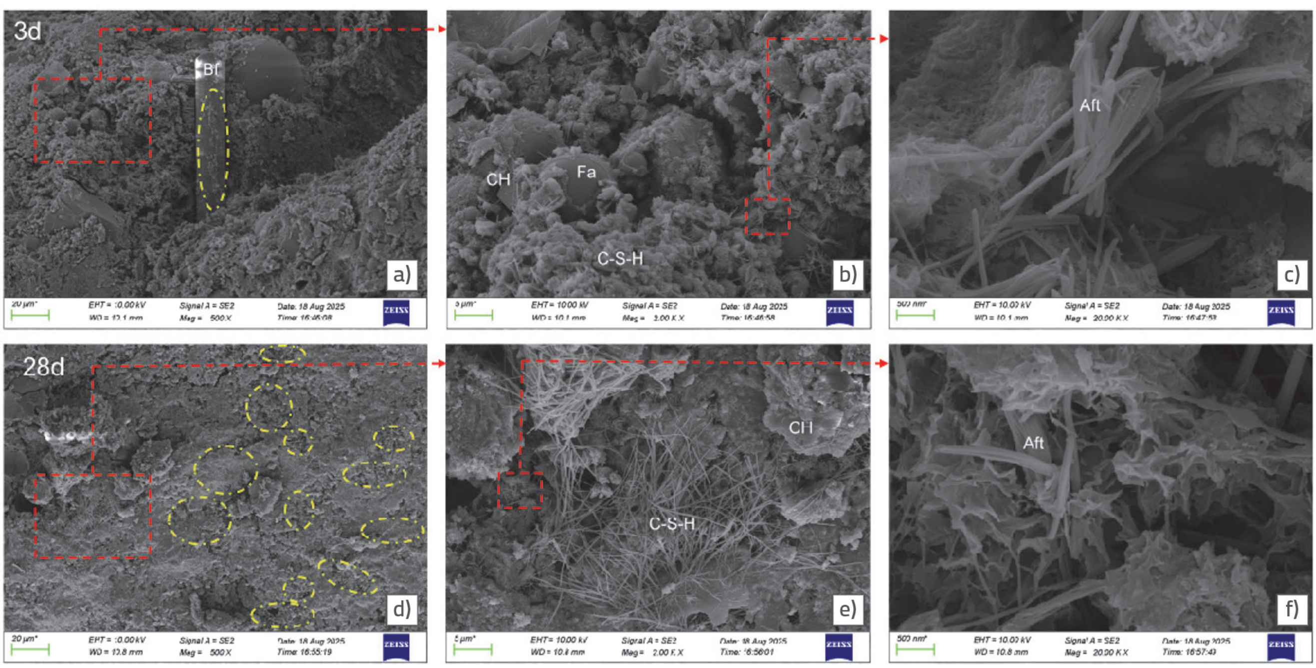

Figure 15. Microstructures of 3d and 28d concrete samples: A1B2C2D2 (Aft: Ettringite; Bf: Basalt fibre; CH: Calcium hydroxide; C-S-H: Calcium silicate hydrate; Fa: Fly ash)

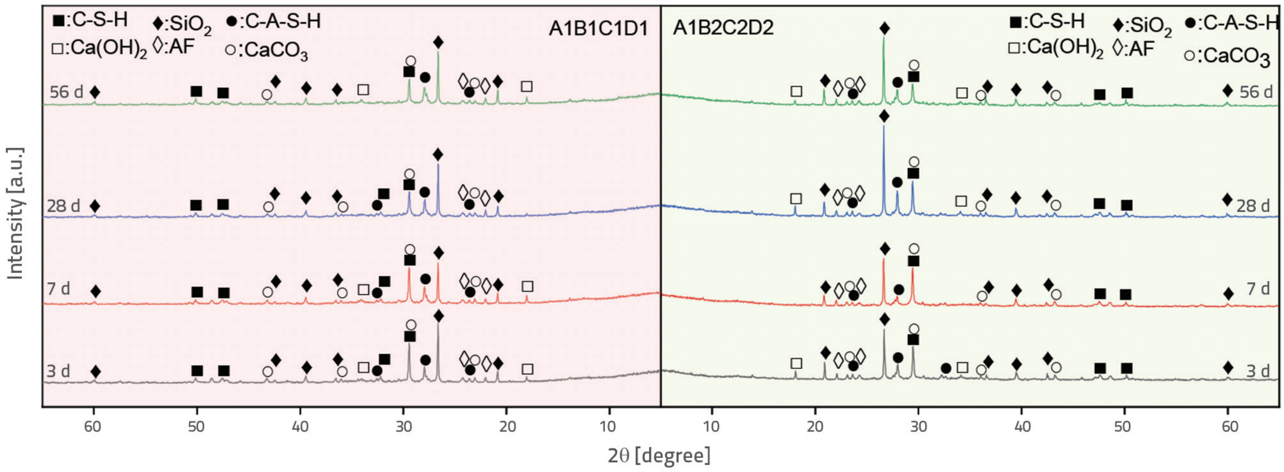

Figure 16. XRD diffraction pattern: A1B1C1D1 and A1B2C2D2

more abundant at 28 day than at 3 day. In the locally enlarged image in Figure 15.f, a small amount of needle- and rod-shaped Aft is observed, surrounded by a large amount of agglomerated flocculent C-S-H. At this stage, the microstructure was more stable and compact at 28 than that at 3 day.

4.4.2. XRD testing

XRD was conducted to examine the mineral compositions of the first and second groups at 3d, 7d, 28d, and 56d, as illustrated in Figure 16. The identified phases included quartz (SiO_2), ettringite (Aft), calcite ($CaCO_3$), calcium hydroxide ($Ca(OH)_2$), and C-S-H. The overall mineral composition was relatively uniform across both groups; however, the intensities of the diffraction peaks for certain hydration products varied with the curing age. Quartz is extensively dispersed across the two sample groups, as shown in Figure 16. At 28 and 56 day, the diffraction peak intensities of the second group were markedly greater than those of the first group, whereas at 3 and 7 day, the intensities were similar. The second group contained higher proportions of fly ash, desert sand, and basalt fibre than the first group. Desert sand and basalt fibre did not participate directly in hydration, but fly ash contributed to its pozzolanic activity. A comprehensive analysis indicated that the concentration of calcium hydroxide in the slurry was relatively low during the early hydration stage. Over time, the pozzolanic effect of fly ash became more pronounced [51] as the fly ash reacted with calcium hydroxide to produce additional C-S-H, thereby densifying the microstructure. In the first group, the diffraction peaks of calcium hydroxide essentially vanished after 28 days, as calcium hydroxide reacted with atmospheric CO_2 to form calcite. In the second group, this transformation occurred earlier at 7 day.

5. Conclusion

In this study, DSBFC was prepared by mixing fly ash, cement, river sand, desert sand, and basalt fibre as raw materials, and its mechanical properties were tested and analysed through 16 groups of orthogonal tests. The following conclusions were drawn:

- The compressive, flexural, and splitting tensile strengths of DSBFC gradually decreased with increasing W/C, FA, DS, and BF. Among the four factors, W/C and FA exerted the most significant influences, whereas DS had the least influence.
- When sheet-like bundles of BF were mixed into the concrete, these bundles gradually separated into monofilaments during mixing and were uniformly dispersed throughout the concrete paste. Under external loading, cracks were initiated in the matrix and propagated to the fracture surface, followed by the pulling-out of monofilament fibres, ultimately leading to strength loss.
- Optimal mix parameters were determined as: W/C = 0.50, FA = 5 %, DS = 10 %, and BF = 0.5 $kg\cdot m^{-3}$. Under these conditions, the compressive strength reached 61.1 MPa, flexural strength 3.77 MPa, and splitting tensile strength 5.01 MPa. Compared with ordinary concrete, this composition reduces river sand usage by approximately 10 % and significantly increases desert sand utilisation, thereby reducing damage to river ecology.

These results highlight the suitability of basalt fibre reinforcement for hydraulic structures and validate the feasibility of using desert sand in concrete for hydraulic engineering applications. Employing desert sand from Xinjiang's desertified regions to build water conservation and irrigation facilities could reduce dependence on river sand mining and lower construction costs. Given the complex natural environment of Xinjiang, further research is required to assess the durability of DSBFC under high salinity, freezing, and large temperature variations. Such studies provide a foundation for large-scale desertification remediation in this region.

Acknowledgements

This study was funded by the Yili Normal University Special Project for Enhancing Comprehensive Disciplinary Strength (22XKZY25).

REFERENCES

[1] Niu, H.: Research on Water and Soil Conservation and Ecological Landscape Planning Measures in Arid Desert Area of Xinjiang - A Case Study on Reservoir Project of Poplar River Town of Tacheng, Xinjiang Agricultural University, Urumqi, China, 2017.

[2] Han, Q.: Evaluation of Fragile Environment and Study of Topical Region, Xinjiang University, Urumi, China, 2005.

[3] Abudourousuli, D.: Analysis of the Bacteria and Archaea Diversity of Saline-Alkaline Soil of Four Sites in Xinjiang, Xinjiang Normal University, Urumqi, China, 2022.

[4] Yao, Y., Zhang, C., Luo, G., Lin, T.: Research on water supply and agricultural water use forecasting in arid regions: a case study of Xinjiang, Frontiers in Environmental Science, 13 (2025), https://doi.org/ 10.3389/fenvs.2025.1578528.

[5] Yang, Y., Wen, Y., Liu, X., Zhao, J., Liu, Q.: Case studies of earthen structures for hydraulic projects damaged under low confining stress during earthquake, Yantu Lixue / Rock and Soil Mechanics, 33 (2012) 9, pp. 2729-2735, 2742.

[6] Weng, Q., Lin, Y., Qin, W.: Recent researches on damage mechanism and penetrability of concrete structure subjected to hydraulic pressure, Cailiao Daobao / Materials Review, 30 (2016) 12, pp. 104-108, 133, https://doi.org/ 10.11896/j.issn.1005-023X.2016.23.015.

[7] Shao, K., Wang, T., Wu, M.: Abrasion Damage of Concrete for Hydraulic Structures after Exposure to Freeze-Thaw Cycles, In IOP Conference Series: Earth and Environmental Science, 1450 (2025), Article 012001, https://doi.org/ 10.1088/1755-1315/1450/1/012001.

[8] Ma, Y., Jiang, X., Li, J., Li, G., Huang, W., Chang, W., Cao, G., Yu, Z.: Research on the Classification of Concrete Sulfate Erosion Types in Tumushuke Area, Xinjiang, Buildings, 14 (2024) 3, Article 729, https://doi.org/ 10.3390/buildings14030729.

[9] Liu, Q., Andersen, L.V., Zhang, M., Wu, M.: Abrasion damage of concrete for hydraulic structures and mitigation measures: A comprehensive review, Construction and Building Materials, 422 (2024), Article 135754, https://doi.org/ 10.1016/j.conbuildmat.2024.135754.

[10] Prasad, P., Tumu, D.B.N., Singh, A., Singh, M.: Effect of different parameters on mechanical properties of basalt fiber based green composites - A critical review, AIP Conference Proceedings, 2962 (2024) 1, pp. 1-5, https://doi.org/ 10.1063/5.0192248.

[11] Jamshaid, H., Mishra, R.: A green material from rock: basalt fiber—a review, Journal of the Textile Institute, 107 (2016) 7, pp. 923-937, https://doi.org/ 10.1080/00405000.2015.1071940.

[12] Li, Y., Shen, A., Guo, Y.: Effect of the addition of basalt fiber on life-cycle anti-cracking behavior of concrete, Archives of Civil and Mechanical Engineering, 23 (2023) 2, Article 92, https://doi.org/ 10.1007/s43452-023-00621-x.

[13] Liang, N., Geng, S., Mao, J., Liu, X., Zhou, X.: Investigation on cracking resistance mechanism of basalt-polypropylene fiber reinforced concrete based on SEM test, Construction and Building Materials, 411 (2024), Article 134102, https://doi.org/ 10.1016/j.conbuildmat.2023.134102.

[14] Wang, X., He, J., Mosallam, A.S., Li, C., Xin, H.: The effects of fiber length and volume on material properties and crack resistance of basalt fiber reinforced concrete (BFRC), Advances in Materials Science and Engineering, (2019), Article ID 7520549, pp. 1-17, https://doi.org/ 10.1155/2019/7520549.

[15] Huang, J., Chen, H.: The influence of basalt fiber length on the mechanical properties and frost resistance of concrete, Journal of Functional Materials, 56 (2025) 3, pp. 3194-3201, https://doi.org/ 10.3969/j.issn.1001-9731.2025.03.025.

[16] Qin, S., Wu, L.: Study on mechanical properties and mechanism of new basalt fiber reinforced concrete, Case Studies in Construction Materials, 22 (2025), Article e04290, https://doi.org/ 10.1016/j.cscm.2025.e04290.

[17] Krassowska, J.: Fracture behavior and mechanical properties of basalt chopped fibers and minibars fiber-reinforced concrete, Structures, 75 (2025), Article 108808, https://doi.org/ 10.1016/j.istruc.2025.108808.

[18] Wang, X., Li, L., Wei, M., Xiang, Y., Wu, Y., Zhou, B., Sun, Y., Cheng, W.: Experimental study on the mechanical properties of short-cut basalt fiber reinforced concrete under large eccentric compression, Scientific Reports, 15 (2025) 1, Article 10845, https://doi.org/ 10.1038/s41598-025-94964-5.

[19] Bao, S., Wang, S., Xia, H., Liu, K., Tang, X., Jin, P.: Enhancing the Mechanical Properties of Recycled Aggregate Concrete: A Comparative Study of Basalt- and Glass-Fiber Reinforcements, Buildings, 15 (2025) 10, Article 1718, https://doi.org/ 10.3390/buildings15101718.

[20] Chang, C., Ning, H., Song, M., Ma, Y., Wang, X., Ketekun, B.T., Kawkabi, K.W., Long, X.: Enhancing mechanical properties of high-strength recycled concrete with basalt fiber and nano-calcium carbonate: Experimental and numerical investigations, Construction and Building Materials, 489 (2025), Article 142264, https://doi.org/ 10.1016/j.conbuildmat.2025.142264.

[21] Lei, T., Qiu, J., Li, L., Huo, Y., Zhang, T.: Study on properties of basalt fiber coal gangue concrete modified by supplementary cementitious materials: Mechanics, durability, microstructure, Journal of Building Engineering, 104 (2025), Article 112271, https://doi.org/ 10.1016/j.jobe.2025.112271.

[22] Xiao, J., Zhou, Y., Deng, Z., Yang, H., Mei, J., Jiang, J., Wei, T.: Investigation of biaxial compressive mechanical properties and strength criteria of basalt fiber-reinforced coral aggregate concrete, Construction and Building Materials, 475 (2025), Article 141199, https://doi.org/ 10.1016/j.conbuildmat.2025.141199.

[23] Bodur, B., Benli, A., Bayraktar, O.Y., Alcan, H.G., Kaplan, G., Aydın, A.C.: Impact of attapulgite and basalt fiber additions on the performance of pumice-based foam concrete: mechanical, thermal, and durability properties, Archives of Civil and Mechanical Engineering, 25 (2025) 2, pp. 1-25, https://doi.org/ 10.1007/ s43452-025-01128-3.

[24] Chen, J.: The Experimental Research on Mix Proportion of Sand Concrete in Gurbantunggut Desert, Shihezi University, Shihezi, China, 2017.

[25] Hamada, H.M., Abed, F., Al-Sadoon, Z.A., Elnassar, Z., Hassan, A.: The use of treated desert sand in sustainable concrete: A mechanical and microstructure study, Journal of Building Engineering, 79 (2023), Article 107843, https://doi.org/ 10.1016/j.jobe.2023.107843.

[26] Liao, T., Huang, X., Yuan, J., Ren, S., Cai, H., Chen, X.: Effects of Desert Sand Substitution on Concrete Properties Using Desert Sand-doped Artificial Sand as the Fine Aggregate, Ceramics-Silikáty, 66 (2022) 4, pp. 540-554, https://doi.org/ 10.13168/ cs.2022.0050.

[27] Zhang, M., Hu, P., Sun, S., Yao, J., Sun, Y., Zhong, J.: Ultra-high-performance alkali-activated concrete produced with desert sand incorporations, Construction and Building Materials, 476 (2025), Article 141240, https://doi.org/ 10.1016/j.conbuildmat.2025.141240.

[28] Xu, W., Liu, H., Qin, D., Doh, S.I.: Study on the mechanical properties of desert sand concrete under dry-wet cycles with sulfate erosion, Physics and Chemistry of the Earth, 138 (2025), Article 103852, https://doi.org/ 10.1016/j.pce.2025.103852.

[29] Munir, M.J., Kazmi, S.M.S., Wu, Y.-F.: High-strength compression-cast desert sand concrete: Stress-strain behavior, durability, microstructure, and cement savings, Journal of Building Engineering, 111 (2025), Article 113284, https://doi.org/ 10.1016/j.jobe.2025.113284.

[30] Rahmani, F., Kaci, S., Ouali, M.O.: On the use of self-compacting concrete based on desert sand and granite powder, Cement, Wapno, Beton, 29 (2024) 3, pp. 171-187, https://doi.org/ 10.32047/CWB.2024.29.3.2.

[31] Hou, L., Jian, S., Huang, W.: The Effect of Polypropylene Fiber and Glass Fiber on the Frost Resistance of Desert Sand Concrete, KSCE Journal of Civil Engineering, 28 (2024) 1, pp. 342-353, https://doi.org/ 10.1007/s12205-023-0694-8.

[32] Qin, Y., Zhang, L., Qu, C., Luo, L.: Flexural mechanical properties of steel fiber desert sand concrete beams, Acta Materiae Compositae Sinica, 39 (2022) 11, pp. 5599-5610, https://doi.org/ 10.13801/j.cnki.fhclxb.20211206.002.

[33] Yu, R., Huang, Y., Sun, J., Liu, Y., Li, S., Luo, S., Liu, Z.: Properties of Steel Fiber Reinforced Desert Sand Concrete, Materials Science Forum, 1131 (2024), pp. 85-98.

[34] Natarajan, R.G., Shanmugamoorthy, S., Veerasamy, S., John, A.: Flexural behavior of sustainable high volume fly ash reinforced concrete beam, GRAĐEVINAR, 77 (2025) 1, pp. 13-25, https://doi.org/ 10.14256/JCE.3830.2023.

[35] Ayyadurai, A., Muthuchamy Maruthai, S., Muthu, D.: Impact of fly ash and banana fiber on mechanical performance of paver block concrete, GRAĐEVINAR, 76 (2024) 3, pp. 211-222, https://doi.org/ 10.14256/JCE.3873.2023.

[36] Zehra, F.A., Soner, G.: Structural self-compacting lightweight concrete: Effects of fly ash and basalt fibers on workability, thermal and mechanical properties under ambient conditions and high temperatures, Construction and Building Materials, 481 (2025), Article 141658, https://doi.org/ 10.1016/j.conbuildmat.2025.141658.

[37] Li, Y., Liu, Y., Zhang, W.: Mechanical, chloride resistance, and microstructural properties of basalt fiber-reinforced fly ash-silica fume composite concrete, Minerals, 15 (2025) 4, Article 348, https://doi.org/ 10.3390/min15040348.

[38] Hamada, H., Abed, F.: Optimization and modeling of 7-day ultra-high-performance concrete comprising desert sand and supplementary cementitious materials using response surface methodology, Buildings, 14 (2024) 7, Article 2058, https://doi.org/ 10.3390/buildings14072058.

[39] Zhang, S., Yuan, K., Zhang, J., Guo, J.: Experimental study on performance influencing factors and reasonable mixture ratio of desert sand ceramsite lightweight aggregate concrete, Advances in Civil Engineering, (2020), Article ID 8613932, pp. 1-9, https://doi.org/ 10.1155/2020/8613932.

[40] Ministry of Housing and Urban-Rural Development of China: standard for technical requirements and test method of sand and crushed stone (or gravel) for ordinary concrete, JGJ 52, Beijing, 2006.

[41] ASTM International: Standard Specification for Concrete Aggregates, ASTM C33/C33M, ASTM International, West Conshohocken, PA, 2016.

[42] Gu, B., Li, Q., Li, C., Zhao, P., Hou, P., Chen, H., Wang, Y., Zhao, P., Cheng, X.: Optimization design of ultra-fine supplementary cementitious materials ultra-high performance concrete mix proportion based on orthogonal experiment, Construction and Building Materials, 453 (2024), Article 139018, https://doi.org/ 10.1016/j.conbuildmat.2024.139018.

[43] Ministry of Housing and Urban-Rural Development of China: specification for mix proportion design of ordinary concrete, JGJ 55, Beijing, 2011.

[44] Ministry of Water Resources of China: Test Code for Hydraulic Concrete, SL/T 352, Beijing, 2020.

[45] Standardization Administration of China: Standard for Test Method of Performance on Ordinary Fresh Concrete, GB/T 50080, Beijing, 2016.

[46] Hamada, H.M., Abed, F., Al-Sadoon, Z.A., Hassan, A.: Enhancing concrete strength and microstructure with basalt and steel fibers in acid and base environments incorporating desert sand, International Journal of Concrete Structures and Materials, 19 (2025) 1, pp. 1-18, https://doi.org/ 10.1186/s40069-024-00741-5.

[47] Huynh, P.T., Ogawa, Y., Kawai, K., Bui, P.T.: Effect of cement type and water-to-binder ratio on k-value of low-calcium fly ash for concrete compressive strength, Journal of Materials in Civil Engineering, 35 (2023) 11, pp. 1-10, https://doi.org/ 10.1061/ JMCEE7.MTENG-15517.

[48] Nayak, D.K., Abhilash, P.P., Singh, R., Kumar, R., Kumar, V.: Fly ash for sustainable construction: A review of fly ash concrete and its beneficial use case studies, Cleaner Materials, 6 (2022), Article 100143, https://doi.org/ 10.1016/j.clema.2022.100143.

[49] Mohammed, B.H., Sherwani, A.F.H., Faraj, R.H., Qadir, H.H., Younis, K.H.: Mechanical properties and ductility behavior of ultra-high performance fiber reinforced concretes: Effect of low water-to-binder ratios and micro glass fibers, Ain Shams Engineering Journal, 12 (2021) 2, pp. 1557-1567, https://doi.org/ 10.1016/j.asej.2020.11.008.

[50] Trezos, K.G., Sfikas, I.P., Pasios, C.G.: Influence of water-to-binder ratio on top-bar effect and on bond variation across length in self-compacting concrete specimens, Cement and Concrete Composites, 48 (2014), pp. 127-139, https://doi.org/ 10.1016/j.cemconcomp.2013.11.012.

[51] He, J., Sun, C., Wang, X.: Study on the effect of fly ash on mechanical properties and seawater freeze-thaw resistance of seawater sea sand concrete, Buildings, 14 (2024) 7, Article 2191, https://doi.org/ 10.3390/buildings14072191.

[52] Wang, Y., Liu, J.: Theoretical investigation on elastic property evolutions of low volume fly ash concrete, Journal of the American Ceramic Society, 108 (2025) 1, https://doi.org/ 10.1111/jace.20127.

[53] Guo, Y., Zhou, H., Zhang, J., Han, C., Wang, H.: Effects of curing temperature and desert sand replacement rate on compressive strength and pore structure of manufactured sand concrete, Journal of Drainage and Irrigation Machinery Engineering, 43 (2025) 1, pp. 45-52, https://doi.org/ 10.3969/j.issn.1674-8530.23.0241.